Shaping effects of the fiber-drawing on particle-rich silica optical fibers, numerical and experimental study

Manuel Vermillac, Zhuorui Lu, Louis Douteau, Yahya Khoder, Nesrine Aïssa, Hugues Digonnet, Luisa Rocha da Silva, Wilfried Blanc

▶ **To cite this version:**

Manuel Vermillac, Zhuorui Lu, Louis Douteau, Yahya Khoder, Nesrine Aïssa, et al.. Shaping effects of the fiber-drawing on particle-rich silica optical fibers, numerical and experimental study. Fiber Lasers and Glass Photonics: Materials through Applications II, Apr 2020, Online, France. pp.50, ⟨10.1117/12.2554028⟩. ⟨hal-02914982⟩

HAL Id: hal-02914982

https://hal.science/hal-02914982v1

Submitted on 1 Apr 2026

HAL is a multi-disciplinary open access archive for the deposit and dissemination of scientific research documents, whether they are published or not. The documents may come from teaching and research institutions in France or abroad, or from public or private research centers.

L'archive ouverte pluridisciplinaire **HAL**, est destinée au dépôt et à la diffusion de documents scientifiques de niveau recherche, publiés ou non, émanant des établissements d'enseignement et de recherche français ou étrangers, des laboratoires publics ou privés.

Distributed under a Creative Commons CC BY 4.0 - Attribution - International License

Shaping effects of the fiber-drawing on particle-rich silica optical fibers, numerical and experimental study

Vermillac M.[a], Lu Z.[b], Douteau L.[a], Khoder Y.[a], Aissa N.[a], Digonnet H.[a], Rocha da Silva L.[a], and Blanc W.[b]

[a]Ecole Centrale de Nantes, ICI, Institut de Calcul Intensif, 1 rue de la Noë, 44321 Nantes Cedex 3, France
[b]Université Côte d'Azur, Institut de Physique de Nice, site Valrose, CNRS UMR 7010, Parc Valrose, 06108 Nice Cedex 2, France

ABSTRACT

Multiphasic optical fibers are promising systems to developp new optical devices. The main issue for their optimization is the control of the structure of the phases. To improve the structuring capabilities, fiber drawing has been evidenced to modify the size and shape of the multiphasic structure of optical fibers. This possibility comes from the occurence of capillary effects during the flow of the material during the fiber drawing. To use the fiber drawing as a structure tailoring step, the main hindrance is the lack of informations on the physical properties of the systems of interest. To that aim, this article presents the work done to measure these properties. Based on experimental results, the characterization of the flow of the fiber drawing of silica-based optical fibers containing nanoparticles is presented. A numerical model for the simulation of the flow of particles and its validation are detailled. Preliminary results of the deformation of particles of various properties in the flow of the fiber drawing are finally presented, indicating a possible non-newtonian behaviour of the particles.

Keywords: Optical fibers, nanoparticles, capillary effects, deformation, Finite element method

1. INTRODUCTION

Particle-rich and multiphasic optical fibers are of great interest for the development of new optical devices. Indeed, compared to homogeneous optical fibers, the presence of nanoparticles may provide various properties, such as tailoring spectroscopic properties of luminescent ions or modifying light propagation in the media [1–5]. Regarding these applications, in addition to composition, the shape, size and spatial distribution of particles or domains are key parameters to optimize their effects. Recently, the fiber drawing, final step of fabrication of an optical fiber, has been evidenced to induce strong modifications of the structure of particles/domains compared to the parent optical preform [6, 7].

During the fiber drawing, the heated material of the optical preform is viscous and flows. During this flow, the particles or domains present inside the material undergo capillary effects, a competition between the viscous stresses of the flow and the surface tension of the interfaces [7]. This dynamic is usually quantified by the capillary number, $\mathrm{Ca}=\eta\dot{\epsilon}R/\gamma$, with η the viscosity of the material, $\dot{\epsilon}$ the deformation rate of the material, R the radius of the particle and γ the surface tension coefficient of the interface. Also important, are the viscosity ratio $\lambda=\eta_p/\eta_m$, viscosity of the particle η_p divided by the viscosity of the matrix η_m, and the nature and evolution of the flow (*e.g.*, extensional, stationnary...). Based on these physical properties, several studies characterized the evolution of particles in simple stationnary flows [8–12]. However, in the case of the fiber drawing, surface tension, viscosity ratios and material behaviours are unknown. This lack of data impedes the prediction of the evolution of the particles in the flow.

Our work focuses on assessing the structuring abilities of capillary effects that occur during the fiber drawing. To that end, our strategy first lies in determining the physical properties of our glass systems, a mandatory knowledge to enable this study. Following this strategy, the viscous stresses of the fiber drawing, $\eta\dot{\epsilon}$, will be

Further author information: (Send correspondence to Vermillac M.)
Vermillac M.: E-mail: manuel.vermillac@ec-nantes.fr

characterized experimentally. Analysis of the neck-down region will be performed to retrieve the evolution of the viscosity and the deformation rate. Then, the use of a numerical model and simulations will be presented, as a mean to assess the physical parameters of our systems (material features). By comparing experimental and numerical results, it would be possible to determine the surface tension stresses σ/R. Numerical methods and validations will be presented, and finally, preliminary results will be discussed.

2. EXPERIMENTAL PART

Experimental procedure

A silica-based optical preform was fabricated following the MCVD process (Modified Chemical Vapor Deposition) [13] to match the fabrication of the fiber sample 1 of Ref. [6]. The porous silica core was doped with GeO_2 and underwent 3 evaporating doping of 5 mL of an ethanol-based solution containg 0.1 mol.L^{-1} of $MgCl_2$ and 10^{-4} mol.L^{-1} of $ErCl_3$ [2]. The optical preform was then fiber drawn in standard conditions at a temperature of approximately 1950 °C, a drawing tension of around 0.28 N and a drawing speed of 0.36 m.s^{-1}. The fiber was coated with a UV-curable polymer (Desolite 3471-3-14, DSM). The diameter of the uncoated fiber was 125 μm.

The neck-down region, the part of the material which extends from preform to fiber, was analyzed to measure the flow of the fiber drawing. To diminish alteration of its shape, at the end of the fiber drawing, the temperature was quickly diminished after the drawing tension ceased to be applied. The neck-down region (also named 'fiber cone' in this article) was then analyzed by SEM (Scanning Electron Microscopy). Around 13 cm of the region of interest of the fiber cone were selected. Due to the finite size of the SEM sample chamber, the fiber cone sample was cut in two pieces.

The SEM results were segmented to obtain the edge of the fiber cone [14]. The longitudinal evolution of diameter was recovered as the maximal distance between the edges, normal to the longitudinal axis of the fiber, for each longitudinal position. The evolution of the radius was then fitted for the two parts of the fiber cone. The fiber side of the cone was arbitrarly fitted with an exponential function. The preform side was arbitrarly fitted with a tenth-degree polynomial function. The first 2 polynomial coefficients were chosen to insure the continuity of the radius and its derivative, with respect to the longitudinal position, at the position of the cut of the fiber cone.

2.1 Experimental results and discussions

An optical fiber was fabricated and drawn in agreement with the 0.3 N part of the La3 sample of Ref. [6]. The objective of this fabrication was to determine the flow of the fiber drawing for a nanoparticle doped optical fiber, drawn in standard conditions.

Based on the work of Paek [15], it is possible to determine the viscous stresses, *i.e.*, flow of the fiber drawing, by knowing the drawing tension and speed. Indeed, the deformation rate $\dot{\epsilon}$ is equal to,

$$\dot{\epsilon} = \frac{\partial V(z)}{\partial z} = \frac{F}{3\eta(z)\pi r^2(z)} \tag{1}$$

with z the longitudinal position, V(z) the speed at position z, F the drawing tension, r the radius of the fiber cone and η the viscosity. The viscosity is defined as,

$$\eta(z) = \frac{Fr(z)}{-6Qr'(z)} \tag{2}$$

With Q the flow, experimentally determined as Q=$V_{fiber} \times \pi r_{fiber}^2$. Eq. 1 and Eq. 2, are based on the main approximations that the viscosity of the material is newtonian, the flow is extensional, and the viscosity is radially homogeneous.

In order to measure the evolution of the radius on the fiber cone, the fiber cone was prepared and analyzed as described in part 2. SEM analyses and image treatment allowed to determine the evolution of the radius, which was then fitted. Figure 1 shows the evolution of the fitted radius of the fiber cone with the longitudinal position.

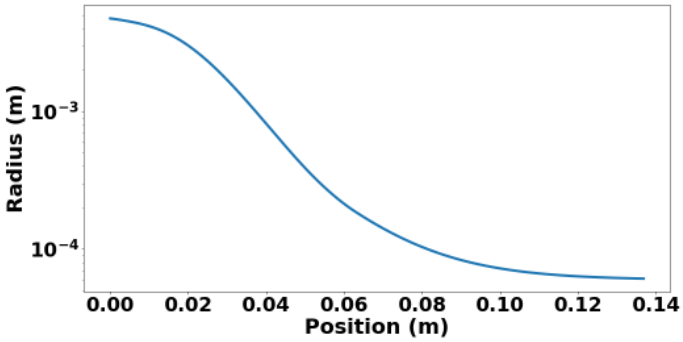

Figure 1. The figure shows in the semilog scale the evolution of the radius of the fiber cone with the longitudinal position, preform side on the left, and fiber side on the right. The radius of the preform side (left side) is close to 0.5 cm and 62 μm on the fiber side (right side).

The junction between the two cut parts of the fiber cone is around the position of 6 cm. It is approximated that there is no abraded part from the cut of the fiber cone.

Then based on the experimental measurements of the drawing speed, and the drawing flow, as well as the radius and its derivative, equations 1 and 2 were used to obtain the viscosity and the deformation rate as a function of the longitudinal position. Left curve of figure 2 shows the evolution of the viscosity in semilog scale as a function of the longitudinal position. Along the analysed part of the fiber cone, inside the furnace, the viscosity first decreases from 10^6 Pa.s to less than 2.10^5 Pa.s in the hot part of the furnace. Then, leaving the hot part, the viscosity increases up to more than 8.10^6 Pa.s. Viscosity is in the same orders of magnitude as found by Paek [15]. The evolution of the deformation rate is plotted on the right curve of figure 2. The deformation rate increases from 10^{-3} s^{-1} up to around 7 s^{-1} and then decreases while getting close to the fiber side. Inflexions points around 6 cm correspond to the location of the cut and junction of the fitted radius functions. Overall,

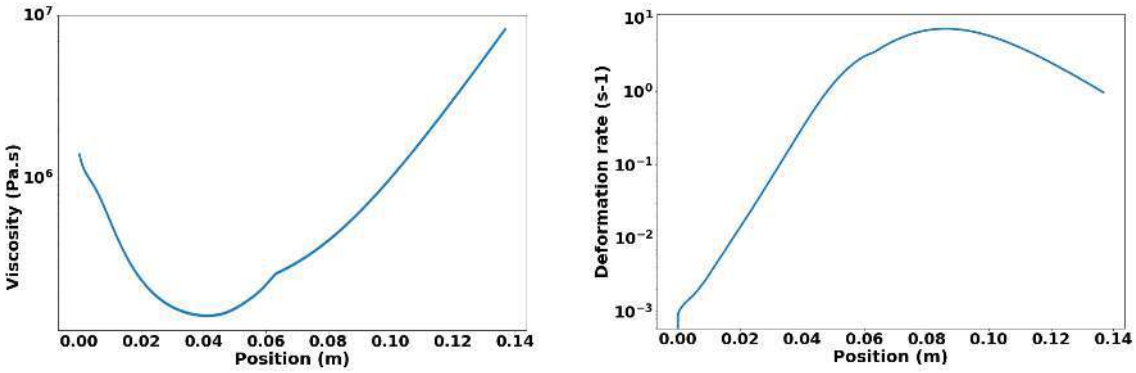

Figure 2. Graphics are in semilog scale and show the evolution of the viscosity (left) and the Deformation rate (right) as a function of the longitudinal position of the fiber drawing cone inside the furnace.

during the fiber drawing, viscosity goes down to around 2.10^5 Pa.s, the deformation rate increases up to around 7 s^{-1}, and it takes approximatively 5 mins for a particle on the preform extremity to reach the fiber extremity.

3. NUMERICAL PART

The flow of the fiber drawing has been characterized and can therefore be used for numerical modelling. The objective is now to run simulations of the deformation of particles of various properties in the flow of the fiber drawing.

3.1 Numerical methodology

The numerical method is based on ICI-tech CFD software, based on the Finite Elements Method (FEM). Considering an incompressible flow of a newtonian fluid in a 3D domain Ω of boundary $\partial\Omega$, Stokes equations are used for conservation of momentum 3 and mass 4 [16]:

$$\eta\nabla^2 v = \nabla p - f \qquad \text{in } \Omega \tag{3}$$

$$\nabla.v = 0 \qquad \text{in } \Omega \tag{4}$$

With $\nabla^2 v$ the laplacian of the velocity, $\nabla.v$ its divergence, ∇ p the pressure gradient, and f the volume forces.

Modeling is done based on the immerse volume method. One set of Stokes equations is solved for the whole domain. The two phases (particle and matrix) are treated as a single fluid with varying local properties [17].

The construction of the fields of properties is done based on the level set approach. Let's consider in the domain Ω, the subdomains of each phases, Ω_p domain of the particle and Ω_m domain of the matrix and their interface Γ. We have,

$$\Omega = \Omega_p + \Omega_m \text{ and } \Omega_p \cap \Omega_m = \Gamma \tag{5}$$

The level set approach enables to represent the interface between the phases and the rest of the domain as the zero level of a signed distance function Φ. For each node at a position $\mathbf{x}$ in the computional domain Ω, by convention, Φ is positive inside the considered phase α (particle or matrix), and negative in the rest of the domain.

$$\Phi_\alpha(x) > 0 \text{ if x } \in \Omega_\alpha \tag{6}$$
$$\Phi_\alpha(x) = 0 \text{ if x } \in \Gamma \tag{7}$$
$$\Phi_\alpha(x) < 0 \text{ if x } \notin \Omega_\alpha \tag{8}$$

To improve numerical stability, the distance function Φ is modified into a smooth distance function Φ_ϵ of thickness ϵ. For each phase α,

$$\Phi_{\epsilon,\alpha} = \epsilon\, tanh(\frac{\Phi_\alpha}{\epsilon}) \tag{9}$$

Then, the smoothed distance function $\Phi_{\epsilon,\alpha}$ is used to build the Heaviside function H.

$$H(\Phi_{\epsilon,\alpha}) = 1 \qquad \text{if } \Phi_{\epsilon,\alpha} > \epsilon \tag{10}$$
$$H(\Phi_{\epsilon,\alpha}) = \frac{1}{2}(1 + \frac{\Phi_{\epsilon,\alpha}}{\epsilon} + \frac{1}{\pi}sin(\frac{\pi\Phi_{\epsilon,\alpha}}{\epsilon})) \qquad \text{if } |\Phi_{\epsilon,\alpha}| < \epsilon \tag{11}$$
$$H(\Phi_{\epsilon,\alpha}) = 0 \qquad \text{if } \Phi_{\epsilon,\alpha} < -\epsilon \tag{12}$$

Heaviside function is used as the support of the mixing law, the law used to specify the properties in the domain. For each node of the computational domain properties are determined as a function of the properties of the particle and matrix, denoted with subscript p and m, respectively :

$$\eta(x) = \eta_m H_m + \eta_p H_p \tag{13}$$
$$H_p = 1 - H_m \tag{14}$$

Surface tension force is expressed as [18],

$$F_{st} = \gamma K n \tag{15}$$

with γ the surface tension coefficient between the phases. n is by convention n_p the gradient of the level set function of the phase of the particle, and K its curvature (by construction, defined at the interface):

$$n_p = \frac{\nabla \Phi_{\epsilon,p}}{\|\nabla \Phi_{\epsilon,p}\|} \tag{16}$$

$$K = -\nabla . n_p \tag{17}$$

Formulation of Finite Elements, is based on volume integrals, whereas surface tension force is a surface force. Therefore, a Dirac function δ is used to integrate the force on the volume:

$$< \delta_\Gamma F, w >= \int_\Gamma \gamma K n . \mathbf{w} = \int_\Omega \delta_\Gamma F_{st} . \mathbf{w} \tag{18}$$

with $\mathbf{w}$ the space of the test functions of the FEM, and δ_Γ the dirac function of the interface Γ, derivative of the smoothed heavisides,

$$\delta_\Gamma = \delta_p = \delta_m = \frac{\partial H_\alpha}{\partial \Phi_{\epsilon,\alpha}} \tag{19}$$

$$\delta(\Phi_{\epsilon,\alpha}) = \frac{1}{2\epsilon}(1 + cos(\frac{\pi \Phi_{\epsilon,\alpha}}{\epsilon})) \qquad if\ |\Phi_{\epsilon,\alpha}| < \epsilon \tag{20}$$

$$\delta(\Phi_{\epsilon,\alpha}) = 0 \qquad if\ |\Phi_{\epsilon,\alpha}| > \epsilon \tag{21}$$

Neglecting the gravity, volume force are equal to surface tension Finally, the level set functions are transported after finding the solution of the Stokes equations:[19]

$$\frac{\partial \Phi_{\epsilon,\alpha}}{\partial t} + v . \nabla \Phi_{\epsilon,\alpha} = 0 \tag{22}$$

$$\tag{23}$$

with t the time. Also discussed in Ref. 19, the advection equation is modified to include a reinitialization algorithm that insures the preservation of the metric properties of the levelset.

To summarize the numerical methodology, from a time t=0, level set functions are used to construct the field of properties (equation 14) and surface tension forces (equation 15). One set of Stokes equations is then solved for the whole domain, giving the velocity field (equations 4 and 3). Then, depending on the numerical time step, level set is transported following equation 23. Time is then incremented and the procedure is repeated until final time of the simulation is reached.

3.2 Numerical validation

Validation of the numerical model, presented in the previous part, was performed on two experimental cases of deformation of particle in flow. The main observable parameter is the aspect ratio of the particle that is defined as the longest center-to-edge distance, L divided by the initial radius of the particle.

The first case is based on the deformation of a particle in shear flow with a capillary number of 0.4, a confinement of 0.5 and a ratio of viscosity of 1 [20, 21]. Confinement is defined as the radius of the particle divided by the length of the domain in the direction of the gradient of velocity. Numerical results shown in

brown on left part of figure 3 agree well with both the experimental results of Sibillo and numerical results of Renardy. Indeed the evolution of the aspect ratio follows well the dynamic and kinetic of the reference cases.

The second case is an extensional flow at a capillary number of 0.187 and a viscosity ratio of 0.056 (viscosity of the particle divided by the viscosity of the matrix) [22]. As for the shear flow case, right part of figure 3 confirms the good agreement between the numerical and experimental results.

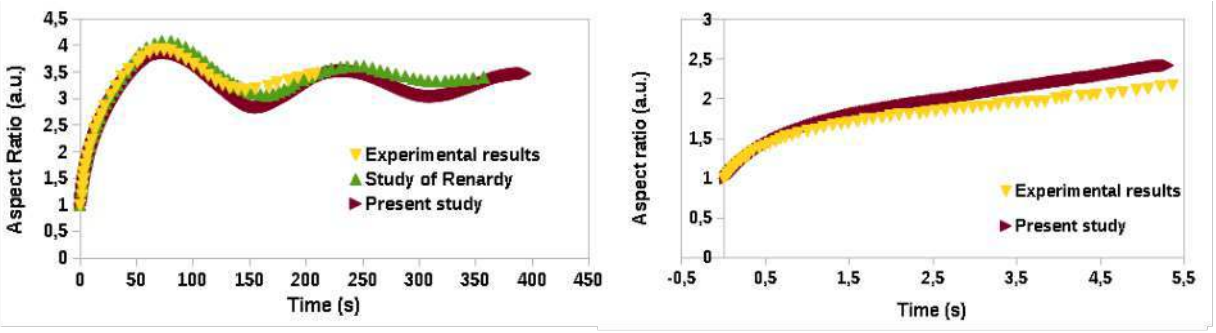

Figure 3. Evolution of the aspect ratio as a function of time for 2 validation cases, shear flow on the left and extensional flow on the right. Shear flow case is done with a capillary number of 0.4, a confinement of 0.5 and a viscosity ratio of 1. Respectively, results in green and yellow correspond to the numerical and experimental results presented in Ref. [20, 21]. Curve in brown corresponds to results of the present study. Extensional flow case is done with a capillary number of 0.187, a confinement of 0.05 and a viscosity ratio of 0.056. Results in yellow and brown correspond to the experimental results presented in Ref [22] and the numerical results of the present study, respectively.

3.3 Preliminary results

After validation of the numerical model, and analysis of the flow of the fiber drawing, simulations of particles in the flow of the fiber drawing have been launched. Although, radius, viscosity and deformation were experimentally characterized as a function of the longitudinal position, it is easier to consider it as a function of time for numerical simulations. As a conversion from longitudinal position, time is recovered for each longitudinal position based an incremental process and volume conservation:

$$t(z=0) = 0 \tag{24}$$

$$t(z+dz) = t(z) + \frac{\pi r^2(z) * dz}{Q} \tag{25}$$

The deformation rate $\dot{\epsilon}$ and viscosities are now functions of time for the simulations. Viscosity of the matrix is defined as the viscosity of the material, and the viscosity of the particle is the viscosity ratio λ multiplied by the viscosity of the material.

$$\eta_m(t) = \eta(t) \tag{26}$$

$$\eta_p(t) = \eta(t) * \lambda \tag{27}$$

3D simulations are made on a domain of 200x20x20 μm with a particle radius of 0.5 μm. 25 cases are launched with viscosity ratios of $\{1;\ 10^{-1};\ 10^{-2};\ 10^{-3};\ 10^{-4}\}$ and surface tension coefficients of $\{0.01;\ 0.03;\ 0.1;\ 0.3;\ 1\}$ N.m^{-1}, to cover a wide range of possible values of both surface tension coefficients [8] and viscosity ratios. First preliminary result is now discussed.

Top image of figure 4 shows an SEM image of a particle inside an optical fiber [6]. Although accuracy is limited, the Q-tips shape of the particle is noticeable. Respectively, second and third image of figure 4 show the shapes of particles that were obtained by numerical simulation of viscosity ratios of 1 and 10^{-4}, and surface tension coefficients of 0.01 N.m^{-1}. The case where λ=1 has typical rounded extremities usually expected for standard deformations of this range of viscosity ratios. The case where λ=10^{-4} also has pointy extremities as

usually expected for this range of viscosity ratios. The fact that no preliminary results of shape correspond to Q-tips shape, might come from the fact that the flow has not been fully undergone. However, it is also possible that it indicates a viscoelastic behaviour of the particle [23].

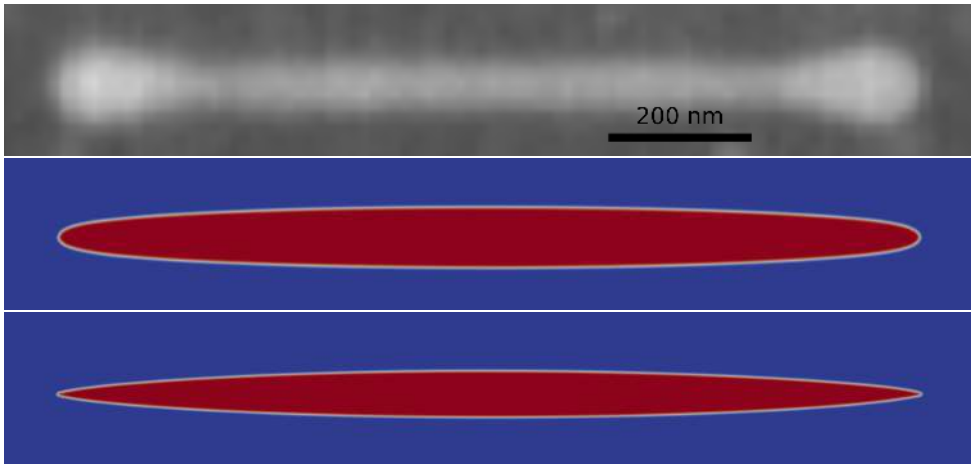

Figure 4. Top image corresponds to a SEM image of a lanthanum rich particle in an optical fiber [6]. The second image corresponds to numerical simulation of a particle that has partially experienced the fiber drawing flow. For the simulation, parameters are a radius of 0.5 μm, a viscosity ratio of 1 and a surface tension coefficient of 0.01 N.m^{-1}. Actual time is 290.3 s over the final time 297.9 s. The second image corresponds to numerical simulation of a particle that has partially experienced the fiber drawing flow. For the simulation, parameters are a radius of 0.5 μm, a viscosity ratio of 10^{-4} and a surface tension coefficient of 0.01 N.m^{-1}. Actual time is 293.4 over the final time 297.9 s.

4. CONCLUSION

In conclusion, multiphasic optical fibers offer new possible properties. One main issue for the improvement of their properties is the control of the structure of the phases. The fiber drawing appears as a good candidate to tailor the shape and size of particles or phase domains. However there is a lack of experimental data on the properties of the materials. This issue impedes the prediction of the evolution of the particles or phases during the fiber drawing. To that aim, the strategy of this work has been presented. First to characterize the flow of the fiber drawing and then to numerically simulate the evolution for particles of various properties, to compare with numerical and experimental data. After analysis of the shape of the fiber drawing cone, the flow of the fiber drawing has been determined based on a newtonian material, and extensional flow approximations. From that flow, simulations of particles of various capillary properties have been launched. Whereas final results of simulations are not available, preliminary results have been discussed. The shape of the extremities of the numerical simulations does not match the Q-tips shape of the particles observed inside the optical fibers. Although this might come from the fact that simulations did not cover the whole flow of the fiber drawing, this observation could highlight a non newtonian behaviour of the particles.

ACKNOWLEDGMENTS

The authors acknowledge S. Trzesien and M. Ude (INPHYNI, Nice, France) for the fabrication of the sample. Authors also thank F. Orange (CCMA, Nice France) for the SEM measurements. This work was supported by ANR project Nanoslim (ANR-17-CE08-0002).

REFERENCES

[1] Veber, A., Lu, Z., Vermillac, M., Pigeonneau, F., Blanc, W., and Petit, L., "Nano-structured optical fibers made of glass-ceramics, and phase separated and metallic particle-containing glasses," *Fibers* **7**(12), 105 (2019).

[2] Vermillac, M., Fneich, H., Lupi, J.-F., Tissot, J.-B., Kucera, C., Vennéguès, P., Mehdi, A., Neuville, D. R., Ballato, J., and Blanc, W., "Use of thulium-doped LaF_3 nanoparticles to lower the phonon energy of the thulium's environment in silica-based optical fibres," *Optical Materials* **68**, 24–28 (2017).

[3] Vermillac, M., Lupi, J.-F., Trzesien, S., Ude, M., and Blanc, W., "On the enlargement of the emission spectra from the $^4I_{13/2}$ level of Er^{3+} in silica-based optical fibers through lanthanum or magnesium co-doping," *Ceramics* **1**(2), 364–374 (2018).

[4] Karbasi, S., Frazier, R. J., Koch, K. W., Hawkins, T., Ballato, J., and Mafi, A., "Image transport through a disordered optical fibre mediated by transverse anderson localization," *Nature communications* **5**(1), 1–9 (2014).

[5] Abaie, B., Mobini, E., Karbasi, S., Hawkins, T., Ballato, J., and Mafi, A., "Random lasing in an anderson localizing optical fiber," *Light: Science & Applications* **6**(8), e17041–e17041 (2017).

[6] Vermillac, M., Fneich, H., Turlier, J., Cabié, M., Kucera, C., Borschneck, D., Peters, F., Vennegues, P., Neisius, T., Chaussedent, S., et al., "On the morphologies of oxides particles in optical fibers: Effect of the drawing tension and composition," *Optical Materials* **87**, 74–79 (2019).

[7] Vermillac, M., Lupi, J.-F., Peters, F., Cabie, M., Vennegues, P., Kucera, C., Neisius, T., Ballato, J., and Blanc, W., "Fiber-draw-induced elongation and break-up of particles inside the core of a silica-based optical fiber," *Journal of the American Ceramic Society* **100**(5), 1814–1819 (2017).

[8] Seward III, T. P., "Elongation and spheroidization of phase-separated particles in glass," *Journal of Non-Crystalline Solids* **15**(3), 487–504 (1974).

[9] Grace, H. P., "Dispersion phenomena in high viscosity immiscible fluid systems and application of static mixers as dispersion devices in such systems," *Chemical Engineering Communications* **14**(3-6), 225–277 (1982).

[10] Taylor, G., "The formation of emulsions in definable fields of flow," *Proceedings of the Royal Society of London. Series A, Containing Papers of a Mathematical and Physical Character* **146**(858), 501–523 (1934).

[11] Stone, H. A., "Dynamics of drop deformation and breakup in viscous fluids," *Annual Review of Fluid Mechanics* **26**(1), 65–102 (1994).

[12] Stone, H. and Leal, L., "The influence of initial deformation on drop breakup in subcritical time-dependent flows at low Reynolds numbers," *Journal of fluid mechanics* **206**, 223–263 (1989).

[13] MacChesney, J., O'connor, P., and Presby, H., "A new technique for the preparation of low-loss and graded-index optical fibers," *Proceedings of the IEEE* **62**(9), 1280–1281 (1974).

[14] Schindelin, J., Arganda-Carreras, I., Frise, E., Kaynig, V., Longair, M., Pietzsch, T., Preibisch, S., Rueden, C., Saalfeld, S., Schmid, B., et al., "Fiji: an open-source platform for biological-image analysis," *Nature methods* **9**(7), 676–682 (2012).

[15] Paek, U. and Runk, R., "Physical behavior of the neck-down region during furnace drawing of silica fibers," *Journal of Applied Physics* **49**(8), 4417–4422 (1978).

[16] https://en.wikipedia.org/wiki/Stokes_flow.

[17] Coupez, T., Digonnet, H., Hachem, E., Laure, P., Silva, L., and Valette, R., "Multidomain finite element computations: Application to multiphasic problems," (2010).

[18] Brackbill, J. U., Kothe, D. B., and Zemach, C., "A continuum method for modeling surface tension," *Journal of computational physics* **100**(2), 335–354 (1992).

[19] Ville, L., Silva, L., and Coupez, T., "Convected level set method for the numerical simulation of fluid buckling," *International Journal for numerical methods in fluids* **66**(3), 324–344 (2011).

[20] Renardy, Y., "The effects of confinement and inertia on the production of droplets," *Rheologica acta* **46**(4), 521–529 (2007).

[21] Sibillo, V., Pasquariello, G., Simeone, M., Cristini, V., and Guido, S., "Drop deformation in microconfined shear flow," *Physical review letters* **97**(5), 054502 (2006).

[22] Ha, J.-W. and Leal, L. G., "An experimental study of drop deformation and breakup in extensional flow at high capillary number," *Physics of fluids* **13**(6), 1568–1576 (2001).

[23] Ramaswamy, S. and Leal, L., "The deformation of a viscoelastic drop subjected to steady uniaxial extensional flow of a newtonian fluid," *Journal of non-newtonian fluid mechanics* **85**(2-3), 127–163 (1999).